ELSEVIER

Ceramics International 31 (2005) 749–755

CERAMICS INTERNATIONAL

www.elsevier.com/locate/ceramint

Microstructure and mechanical properties of liquid-phase-sintered SiC with AlN and Y_2O_3 additions

Keiichiro Suzuki*, Mikio Sasaki[1]

Research Center, Asahi Glass Co., Ltd., Yokohama 221-8755, Japan

Received 19 May 2004; received in revised form 15 June 2004; accepted 2 August 2004
Available online 18 January 2005

Abstract

Pressureless liquid-phase sintering of β-SiC with AlN and Y_2O_3 was investigated to improve its strength property at high temperatures. For the sintered SiC with 1 wt% Y_2O_3, the grain size decreased with an increase in the AlN addition up to 10 wt% and the aspect ratio of the grains increased up to 5 wt% AlN. The densified SiC with 10 wt% AlN and 1 wt% Y_2O_3 additions sintered at 2100 °C for 5 h had flexural strengths of 870 MPa at RT and 755 MPa at 1400 °C. This strength behavior is explained in terms of the microstructure being composed of fine plate-like grains interlocking with very few pores and with a high refractoriness of the grain boundary phase. The fracture toughness of the SiC decreased with increasing AlN addition.
© 2004 Elsevier Ltd and Techna Group S.r.l. All rights reserved.

Keywords: A. Sintering; B. Microstructure-final; C. Strength; D. SiC

1. Introduction

Liquid-phase-sintered silicon carbide (LPS-SiC) has been extensively studied to obtain toughened structural ceramics. Solid-state pressurelessly sintered SiC with additions of boron and carbon has high strength, high corrosion resistance and high hardness from room temperature (RT) to elevated temperatures [1,2]. However, its fracture toughness is relatively low, being 2–3 MPa·$m^{1/2}$, which is approximately half that of sintered silicon nitride due to its substantially transgranular fracture mode, which is a disadvantage for practical applications.

For LPS-SiC various sintering additives have been reported such as Al_2O_3 [3–5], Al_2O_3–Y_2O_3 [6–8], yttrium–aluminum garnet (YAG) [9] and AlN–Y_2O_3 [10–13]. These additives form a liquid during sintering with SiO_2, which is the oxidized surface layer of SiC particles, and the liquid promotes densification and microstructure development through grain rearrangement and solution-reprecipitation. Regarding LPS-SiC, the sintering is more controllable for the purpose of obtaining a homogeneous microstructure with fine grains compared with solid-state sintering, in which exaggerated grain growth often occurs causing a strength decrease. In most cases of pressureless LPS-SiC, the obtained microstructure can consist of plate-like grains with grain boundaries of the second phase resulting in a higher fracture toughness due to crack deflection or crack bridging in intergranular fracture mode. Several attempts to obtain such a microstructure have been reported also for hot-pressing including the use of β-SiC starting powder and the incorporation of α-SiC seeds [14,15], SiC platelet [16] or SiC whisker [17], often accompanied by heat treatments after sintering.

The authors have focused on the study of pressureless LPS-SiC with the addition of Al_2O_3 [3,4,18,19]. We have demonstrated that pressurelessly sintered β-SiC with Al_2O_3 has a microstructure with elongated plate-like SiC grains resulting in a fracture toughness of 5–6 MPa·$m^{1/2}$ [4]. With increasing the sintering time at 1950 °C, the fracture toughness of the SiC increased with increased the aspect ratio of the grains. The Al_2O_3-added SiC has high strength at RT and high oxidation resistance at high temperatures [18]. However, its flexural strength decreases at high tempera-

* Corresponding author.
E-mail address: keiichiro-suzuki@agc.co.jp (K. Suzuki).
[1] Present address: Kansai Factory, Asahi Glass Co., Ltd., Amagasaki 660-0857, Japan. Tel.: +81 45 503 7162; fax: +81 45 503 5179.

0272-8842/$30.00 © 2004 Elsevier Ltd and Techna Group S.r.l. All rights reserved.
doi:10.1016/j.ceramint.2004.08.014

tures, to 50–70% of the RT strength at 1400 °C, whereas the boron-doped SiC does not decrease in strength even at high temperatures. Therefore, we have investigated the possibility of increasing the strength of LPS-SiC at high temperatures.

The possible strategies for increasing the high temperature strength are as follows. (1) Having no grain boundary phase which softens at high temperatures, (2) having a crystallized grain boundary phase with a high refractoriness and (3) having a three-dimensionally well-interlocked elongated grain structure with a very thin glassy grain boundary phase. The possibility of (1) is thought to be difficult when using a liquid, except in the case of solid-state sintering. In the case of pressureless sintering of β-SiC with Al_2O_3, Al_2O_3 decomposes with SiC during sintering and a microstructure of sufficiently elongated plate-like grains interlocking with each other is formed with an extremely thin Al-rich layer of 0.5–1.0 nm thickness at the grain boundaries [19]. This microstructure seems to be very similar to that in (3). Nevertheless, even after optimizing the sintering process followed by gas pressure soaking, the flexural strengths of the SiC fabricated using a commercially available SiC powder were 685 MPa at RT and 485 MPa at 1400 °C, which is 71% of the strength at RT [19]. We have also concentrated on finding better sintering additives and a process which produces a transient liquid for densification, and on making a highly refractive grain boundary crystalline phase in order to achieve (2). After investigating various sintering aids and pressureless sintering conditions we have found that SiC with additions of AlN and Y_2O_3 has a high strength at elevated temperatures [20].

Regarding AlN addition to SiC, many studies on SiC–AlN solid solution [10,21–24] have been presented and several investigations on an AlN sintering additive for hot-pressed SiC [25] with Er_2O_3 [26,27] and for pressureless-sintered SiC with Y_2O_3 [11–13] have been reported. Cutler et al. [21] showed that an extensive solid solution exists between SiC and AlN or aluminum oxycarbide Al_2OC. Studies on the phase relationship, microstructure and properties of the SiC–AlN solid solution have been carried out. No additive is needed for densification of the SiC–AlN solid solution by hot pressing, whereas additives like Y_2O_3 are required for its pressureless sintering. Pressureless-sintered SiC–50%AlN composites with Y_2O_3 showed no strength decrease at temperatures below 1200 °C, but showed a remarkable decrease from 1350 °C [10].

Keppeler et al. [11] investigated the high-temperature mechanical behavior of LPS-SiC with AlN–Y_2O_3 additions. A green body of 1 wt% α-SiC seeds and 99 wt% β-SiC mixed with 10 vol% AlN–Y_2O_3 (3:2 molar ratio) was pressurelessly sintered at 1990 °C for 30 min, followed by gas pressure sintering. The flexural strength of the SiC with a platelet-shaped microstructure was constant between RT and 1000 °C, at 524 MPa, but above 1000 °C, the strength continuously decreased to reach 377 MPa at 1400 °C. The microstructural evolution of SiC with AlN–Y_2O_3 additions of 10 vol%, in which the molar ratio of AlN to Y_2O_3 was from 4:1 to 1:4, was reported by Schneider et al. [13]. They fabricated a fully dense SiC by pressureless sintering without a powder bed. The increased Y_2O_3 content increased the creep resistance due to the higher viscosity of the liquid.

Nakamura and Maeda [25] demonstrated hot-pressed SiC with AlN having the high flexural strength of >1000 MPa from RT to 1600 °C. Kim et al. [26] showed that hot-pressed β-SiC containing 1 wt% α-SiC with AlN and Er_2O_3 has the flexural strength of 550 MPa at 1600 °C, which is 93% of its strength at RT. This high strength at high temperatures was explained by the presence of the grain boundary film with a high refractoriness.

Although many studies on pressureless LPS-SiC have been carried out, the high-temperature flexural strength of SiC above 650 MPa at 1400 °C has not been reported as far as we know. In this study, the pressureless sintering of β-SiC alone with AlN and Y_2O_3 additions was investigated in order to obtain LPS-SiC with high flexural strength at high temperatures. The microstructure depending on the AlN and Y_2O_3 additive amounts, and the relations between the microstructures and the mechanical properties are reported.

2. Experimental procedure

The starting materials for this study were β-SiC (Ibiden Corp., Gifu, Japan, Betarundum-Ultrafine), AlN (H.C. Starck, Berlin, Germany) and Y_2O_3 (Shin-Etsu Chemical Co., Tokyo, Japan, 99.5% pure). The investigated compositions are listed in Table 1. The mixtures of SiC, AlN and Y_2O_3 powders were ball-milled for 24 h in a plastic jar with SiC balls and ethanol. The dried powders were uniaxially pressed in a steel die under 20 MPa into 15 mm × 20 mm × 40 mm or 15 mm × 40 mm × 70 mm rectangular samples.

Table 1
Compositions of the samples for SiC with AlN and Y_2O_3 additions

Powder	wt%															
	Sample denotation															
	A5	A10	A15	A20	A1Y1	A2Y1	A5Y1	A10Y1	A15Y1	A20Y1	A5Y5	A10Y5	A15Y5	A20Y5	A5Y10	A10Y10
SiC	95	90	85	80	98	97	94	89	84	79	90	85	80	75	85	80
AlN	5	10	15	20	1	2	5	10	15	20	5	10	15	20	5	10
Y_2O_3	0	0	0	0	1	1	1	1	1	1	5	5	5	5	10	10

Subsequently the samples were isostatically pressed under 200 MPa.

The sintering was performed using a graphite resistance furnace. The green compacts were embedded in a powder bed in a graphite container with a lid. The powder bed used was a mixture of 80 wt% graphite grit (Toyo Carbon Co., Japan, particle size: <3 mm, purity: 98–99%,) and 20 wt% Al_2O_3 powder (Sumitomo Aluminum Co., Japan, A-21). The sintering conditions were (a) 2100 °C, 4 h, Ar and (b) 2100 °C, 5 h, N_2. For (a) the samples of 15 mm × 20 mm × 40 mm size were used, whereas for (b), those of 15 mm × 40 mm × 70 mm size were used. The heating rate was 400 °C/h; the samples were heated in vacuum up to 1000 °C and in an atmosphere of Ar or N_2 above 1000 °C.

The bulk densities of the sintered bodies were measured by the Archimedes method. Theoretical densities were determined by the rule of mixtures, using the starting compositions to calculate the relative densities. The sintered samples were cut to 3 mm × 3 mm × 30 mm eliminating the as-sintered surface and the cut surfaces were mirror polished to enable the characterization and measurements of mechanical properties.

Characterization was performed for selected sintered samples (A1Y1, A2Y1, A5Y1 and A10Y1). The microstructures were observed using a scanning electron microscope (SEM) for the polished and chemically etched surfaces. The SEM images were analyzed using an image processing software, NIH Image, which is in the public domain. The mean grain size and the mean aspect ratio of grains were calculated from 150 to 200 grains in each case. The mean pore size and the pore density were also determined for pores of above 0.5 μm diameter on the polished surfaces.

X-ray diffraction using Cu Kα radiation was conducted on the polished surfaces of the specimens. The contents of Al and Y in the sintered bodies were analyzed for the ground samples using an Inductively Coupled Plasma (ICP) spectrometer and the contents of O and C were determined by a selective hot-gas extraction method. The solute contents of Al and Y in the ground samples in a HF–HNO_3 solution were also analyzed using ICP to evaluate the grain boundary phase.

A three-point flexural strength measurement was carried out using the test bars (3 mm × 3 mm × 30 mm) at a crosshead speed of 0.5 mm/min with a span of 20 mm. Three or four bars of each sintered sample were tested at RT and 1400 °C. The fracture toughness measurement was performed at RT by an indentation fracture method [28]. The fracture toughness K_{IC} is given by

$$K_{IC} = 0.018\left(\frac{E}{H}\right)^{1/2}\left(\frac{P}{C^{3/2}}\right)$$

where E is Young's modulus, H is Vicker's hardness, P is indent load, and C is half of the indentation crack length. In this study, E = 423 GPa, which was obtained in our other study, and P = 196 N were used.

3. Results and discussion

Table 2 shows the relative densities of the sintered samples. The samples had above 94% density except A5. An addition of Y_2O_3 of at least 1 wt% with AlN was effective in increasing the density. The highest density of 98.2% was obtained for A10Y1 sample sintered in Ar, but the density of its cut specimen without the as-sintered surface was 99.8%. The larger the additive amount, the higher its real relative density must be, because of the decomposition of the additive constituents during sintering as described below. The densities of the samples sintered in N_2 were lower than those sintered in Ar. This can be explained by the fact that the liquid viscosity would be higher in N_2 [29] and the samples sintered in N_2 were larger than those sintered in Ar.

The typical microstructures of A1Y1, A2Y1, A5Y1 and A10Y1 sintered in Ar are shown in Fig. 1. The mean grain size and the aspect ratio of the grains are shown as a function of AlN addition in Fig. 2. Upon increasing the AlN addition from 1 to 10 wt% the mean grain size decreased. The grain shape changed from substantially globular to elongated plate-like, and the mean aspect ratio increased from 1.6 to 3.5 with increased AlN addition in the range from 1 to 5 wt%. Fig. 3 shows the pore size and the pore density in the samples as a function of AlN addition. The mean pore size decreased with increasing AlN addition, whereas the pore density had a maximum at 2 wt% AlN and decreased above that amount. A10Y1 had the fewest and the smallest pores. Its calculated porosity from the mean pore size and the pore density was 0.05 vol%. These microstructures can be attributed to a larger amount of the liquid which promotes densification through grain rearrangement and grain growth through solution-reprecipitation with increased AlN addition. Jun et al. [30] has reported that a nitrogen-containing liquid inhibits phase transformation and grain growth, from an investigation involving the addition of AlN to SiC with

Table 2
Relative densities of SiC with AlN and Y_2O_3 additions

Sintering condition	(%)															
	A5	A10	A15	A20	A1Y1	A2Y1	A5Y1	A10Y1	A15Y1	A20Y1	A5Y5	A10Y5	A15Y5	A20Y5	A5Y10	A10Y10
(a)					96.2	97.4	97.4	98.2								
(b)	91.2	95.2	96.0	95.7			94.9	97.0	96.6	95.3	94.8	96.8	97.4	95.1	93.9	94.1

(a) 2100 °C, 4 h, Ar; (b) 2100 °C, 5 h, N_2.

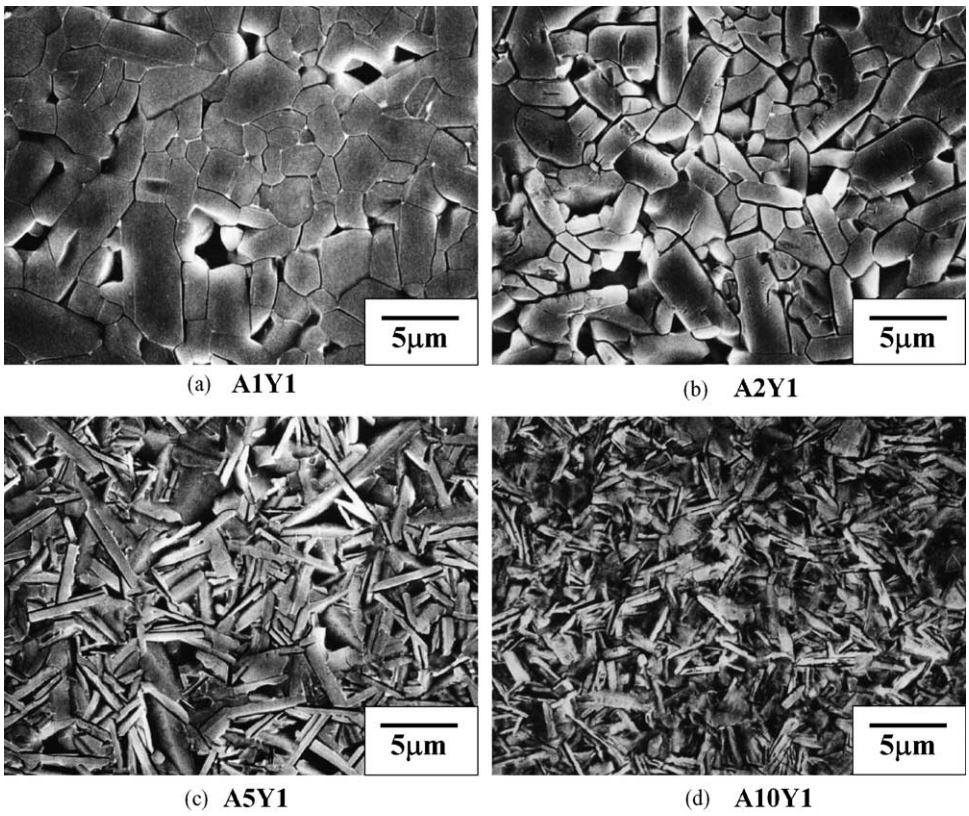

Fig. 1. Typical microstructures of SiC with AlN and Y_2O_3 additions sintered at 2100 °C for 4 h in Ar.

Al_2O_3 and Y_2O_3. The decreasing tendency of the grain size with increased AlN in this study is consistent with their findings.

All X-ray diffraction patterns of A1Y1, A2Y1, A5Y1 and A10Y1 sintered in Ar appeared to correspond with SiC(4H) without any other distinct peaks, indicating that β-SiC(3C) transformed to SiC(4H) through solution-reprecipitation. The value of 2θ for (1 1 0) Cu Kα showed a decrease of 0.22° with increasing the amount of AlN addition from 1 to 10 wt%. The SiC–AlN solid solution (2H) has been reported to have a continuous decrease in the value of 2θ for the (1 1 0) plane from 60.0° of SiC to 59.4° of AlN [22]. Therefore, the decrease in the value of 2θ for (1 1 0) in this study would suggest the formation of a SiC–AlN solid solution. It seems reasonable from the observation of the peak intensities that SiC(4H) decreases and SiC–AlN solid solution increases with the increase in AlN addition.

The total contents of Al, Y, O, N and the solute contents of Al and Y to the $HF–HNO_3$ solution in the sintered samples are shown in Table 3. The Al content did not change

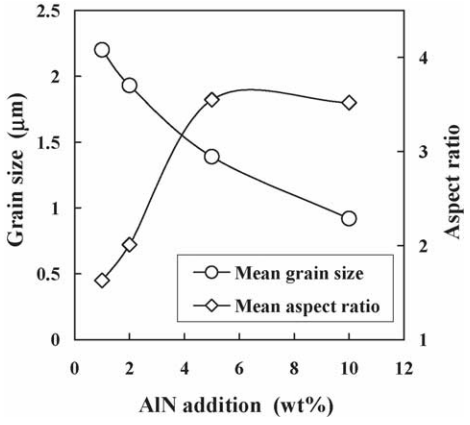

Fig. 2. Mean grain size and mean aspect ratio of SiC with AlN and Y_2O_3 additions (A1Y1, A2Y1, A5Y1 and A10Y1) sintered at 2100 °C for 4 h in Ar, as a function of AlN addition.

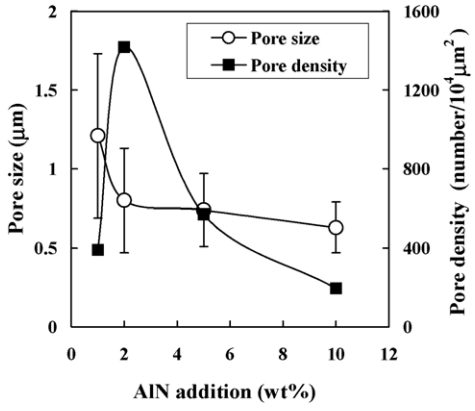

Fig. 3. Pore size and pore density of SiC with AlN and Y_2O_3 additions (A1Y1, A2Y1, A5Y1 and A10Y1) sintered at 2100 °C for 4 h in Ar, as a function of AlN addition.

Table 3
Elemental analysis of SiC with AlN and Y_2O_3

Element		(wt%)			
		A1Y1	A2Y1	A5Y1	A10Y1
Al	total	0.96	1.33	3.22	6.29
	solute	1.00	0.43	1.09	2.27
Y	total	0.08	0.13	0.44	0.50
	solute	0.11	0.10	0.36	0.51
O	total	0.13	0.23	0.78	1.27
N	total	0.19	0.28	0.40	1.10

Sintering conditions: 2100 °C, 4 h, Ar. Total: total content in the sintered specimen. Solute: solute content to HF-HNO_3 solution in the sintered specimen.

in A2Y1, A5Y1 or A10Y1 during sintering, whereas it increased in A1Y1, which could be due to a transfer of constituent Al from the powder bed. In A1Y1 and A2Y1 the contents of Y and O decreased significantly, indicating the decomposition of Y_2O_3. A decrease in N content with AlN addition was observed, suggesting the decomposition of AlN and the vaporization of the N content.

It was found that SiC and Al_2O_3 do not dissolve in the HF–HNO_3 solution. Taking into consideration the fact that the fracture mode is predominantly intergranular under grinding as described below, the solute constituents of the ground samples to the HF–HNO_3 solution would be mainly those of the grain boundary phase. Approximately 100% of the Al content for A1Y1 and 30% of that for A2Y1, A5Y1 and A10Y1 dissolved in the HF–HNO_3 solution, whereas the total Y content dissolved for all four samples. Therefore, it is assumed that the grain boundary phase would contain 30–100% of the Al content and 100% of the Y content of the sintered specimens. Schneider et al. [13] reported that the sintered SiC with AlN and Y_2O_3 has grain boundary phases of $Y_{10}Al_2Si_3O_{18}N_4$ and Y_2O_3. The samples in this study could have a similar grain boundary phase of Y-Si-Al-O-N. The insoluble Al may be a constituent of Al-SiC(4H) and AlN–SiC solid solutions for A2Y1, A5Y1 and A10Y1. SiC(4H) is known to have a solid solubility of Al up to 1 wt% [31]. For A1Y1, SiC is thought not to have a solid solution with Al or AlN, and therefore, the total amounts of Al, Y, O and N might exist in the grain boundary phase.

The flexural strengths at RT and 1400 °C of the sintered SiC are shown as a function of AlN addition in Figs. 4 and 5, respectively. Regarding the SiC sintered at 2100 °C for 4 h in Ar, the strength at RT increased with increased AlN addition up to 5 wt% and the strength at 1400 °C also increased markedly, up to 10 wt%. The latter exceeded 650MPa at AlN addition of 10 wt%. Regarding the SiC sintered at 2100 °C for 5 h in N_2, the strengths at both RT and 1400 °C had maximum values at AlN addition of 10 wt%. The SiC without Y_2O_3 indicated a lower strength at RT in the AlN range from 5 to 15 wt%. The highest flexural strength at 1400 °C in this study was 755 MPa, which is 86.1% of the strength at RT, for the SiC sintered in N_2 with 10 wt% AlN and 1 wt% Y_2O_3.

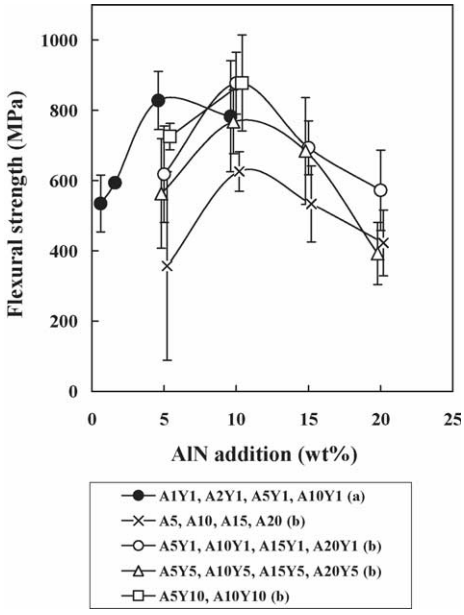

Fig. 4. Flexural strength at RT for SiC with AlN and Y_2O_3 additions, as a function of AlN addition. Sintering conditions: (a) 2100 °C, 4 h, Ar; (b) 2100 °C, 5 h, N_2.

The typical fracture surfaces of the specimens used for the RT flexural strength measurement are shown in Fig. 6 for A1Y1, A2Y1, A5Y1 and A10Y1. They indicate a substantially intergranular fracture mode. It appears that the proportion of transgranular fracture mode increased with increased AlN addition.

The high RT flexural strengths of SiC with 5 and 10 wt% AlN would be due to the small number and size of flaws and the interlocking microstructures having plate-like grains

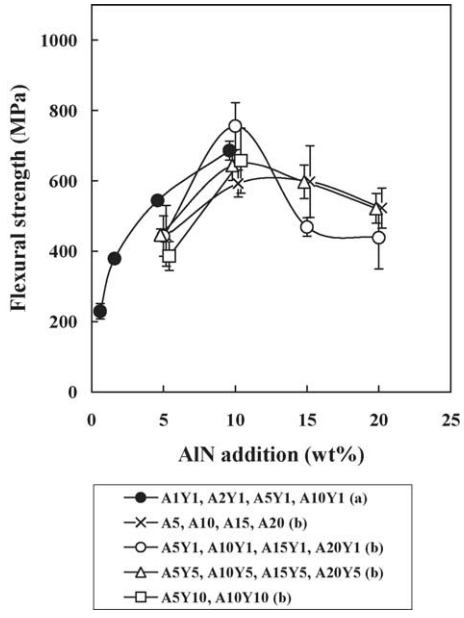

Fig. 5. Flexural strength at 1400 °C for SiC with AlN and Y_2O_3 additions, as a function of AlN addition. Sintering conditions: (a) 2100 °C, 4 h, Ar; (b) 2100 °C, 5 h, N_2.

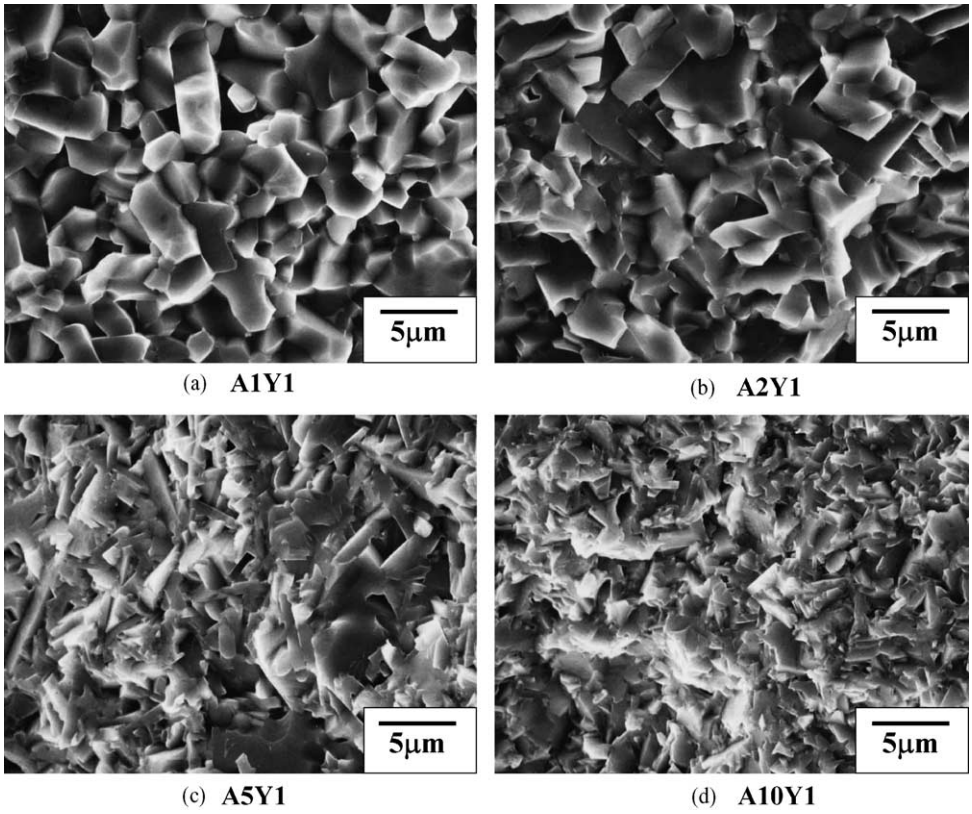

Fig. 6. Typical fracture surfaces of SiC with AlN and Y_2O_3 additions sintered at 2100 °C for 4 h in Ar.

with relatively high aspect ratios. Above 650 MPa, the high flexural strengths at 1400 °C of the SiC with 10 wt% AlN could be attributed to the improved grain boundary phase with heat-resistant crystallized Y-Si-Al-O-N. Further investigation is required to identify the grain boundary phase and clarify its formation process in detail.

Fig. 7 shows the fracture toughness K_{IC} of the SiC sintered at 2100 °C for 4 h in Ar, as a function of AlN addition. K_{IC} decreased from 6.7 to 3.7 MPa·m$^{1/2}$ with increased AlN addition. This tendency is considered to be due to the decrease in the grain size and the increase in trangranular fracture mode, which results in a decrease of the crack tortuosity by crack deflection or bridging. In the SiC sintered in Ar, a trade off tendency is shown between the strength at 1400 °C and the fracture toughness at RT. However, the K_{IC} value of 3.7 MPa·m$^{1/2}$of A10Y1 sintered in Ar could be even higher than 1.5 times that of boron-doped SiC. The fracture toughness of A10Y1 sintered in N_2 was 6.1 MPa·m$^{1/2}$, higher than that of A10Y1 sintered in Ar. When using a N_2 atmosphere, the liquid has a higher viscosity and the weight loss during sintering decreases [29,32]. Therefore, the higher fracture toughness might be due to a thicker grain boundary film which results in an increase in intergranular fracture mode.

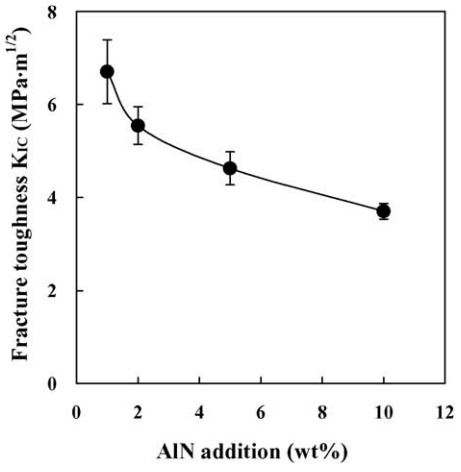

Fig. 7. Fracture toughness of SiC with AlN and Y_2O_3 additions (A1Y1, A2Y1, A5Y1 and A10Y1) sintered at 2100 °C for 4 h in Ar, as a function of AlN addition ($n = 5$).

4. Conclusion

Pressureless LPS-SiC with AlN and Y_2O_3 was investigated, with the aim of obtaining a high strength property at elevated temperatures. As a result, SiC with flexural strengths of 870 MPa at RT and 755 MPa at 1400 °C was obtained in the case of using β-SiC with 10 wt% AlN and 1 wt% Y_2O_3 additions sintered at 2100 °C. Upon increasing the AlN addition from 1 to 10 wt% with the addition of Y_2O_3 being constant at 1 wt%, the grain morphology of the SiC changed from globular to plate-like, with a decreased grain

size and increased aspect ratio. At the same time, the composition changes proceeded accompanied by decreases in N and Y_2O_3 contents and the formation of SiC–AlN solid solution, which would result in a decrease in the grain boundary phase and an increase in its refractoriness. The increase in the high temperature strength is considered to be due to the improvement of the grain boundary phase. The fracture toughness decreased with increased AlN addition. However, the relatively high K_{IC} value of 6.1 MPa·$m^{1/2}$ was obtained for the SiC sintered in N_2. The pressureless-sintered SiC with AlN and Y_2O_3 additions is expected to have a high potential for various structural applications at high temperatures.

Acknowledgements

The authors sincerely thank the staff and researchers at the Research Center of Asahi Glass Co., Ltd. for their support and assistance. Specific acknowledgement is due to Mr. M. Sugizaki for the elemental analysis.

References

[1] S. Prochazka, Sintering of silicon carbide, in: J.J. Burke, A.E. Gorum, R.N. Katz (Eds.), Ceramics for High Performance Applications, Brook Hill Pub. Co., Chestnut Hill, MA, 1974, pp. 239–252.
[2] J.A. Coppola, M. Srinivasan, K.T. Faber, R.H. Smoak, High temperature properties of sintered alpha silicon carbide, in: S. Somiya, S. Saito (Eds.), in: Proceedings of the International Symposium of Factors in Densification and Sintering of Oxide and Non-oxide Ceramics, Gakujutsu Bunka Fukyu-kai, Tokyo, 1979, pp. 400–417.
[3] K. Suzuki, Pressureless sintering of silicon arbide with addition of aluminium oxide, Rep. Res. Lab. Asahi Glass Co. 36 (1) (1986) 25–36.
[4] K. Suzuki, M. Sasaki, Pressureless sintering of silicon carbide, in: S. Somiya, R.C. Bradt (Eds.), Fundamental Structural Ceramics, Terra Scientific Publishing Co., Tokyo, 1987, pp. 75–87.
[5] M.A. Mulla, V.D. Krstic, Pressureless sintering of β-SiC with Al_2O_3 additions, J. Mater. Sci. 29 (1994) 934–938.
[6] M. Omori, H. Takei, Pressureless sintering of silicon carbide, J. Am. Ceram. Soc. 65 (6) (1982) C-92.
[7] M.A. Mulla, V.D. Krstic, Low-temperature pressureless sintering of β-silicon carbide with aluminum oxide and yttrium oxide additions, Am. Ceram. Soc. Bull. 70 (3) (1991) 439–443.
[8] N.P. Padture, In situ-toughened silicon carbide, J. Am. Ceram. Soc. 77 (2) (1994) 519–523.
[9] L.S. Sigl, H.J. Kleebe, Core/rim structure of liquid-phase-sintered silicon carbide, J. Am. Ceram. Soc. 76 (3) (1993) 773–776.
[10] J.-F. Li, R. Watanabe, Pressureless sintering and high-temperature strength of SiC–AlN ceramics, J. Ceram. Soc. Jpn. 102 (8) (1994) 727–731.
[11] M. Keppeler, H.-G. Reichert, J.M. Broadley, G. Thurn, I. Wiedmann, F. Aldinger, High temperature mechanical behaviour of liquid phase sintered silicon carbide, J. Eur. Ceram. Soc. 18 (1998) 521–526.
[12] M. Nader, F. Aldinger, M.J. Hoffmann, Influence of the α/β-SiC phase transformation on microstructural development and mechanical properties of liquid phase sintered silicon carbide, J. Mater. Sci. 34 (1999) 1197–1204.
[13] J. Schneider, K. Biswas, G. Rixecker, F. Aldinger, Microstructural changes in liquid-phase-sintered silicon carbide during creep in an oxidizing environment, J. Am. Ceram. Soc. 86 (3) (2003) 501–507.
[14] G.-D. Zahn, M. Mitomo, H. Tanaka, Y.-W. Kim, Effect of annealing conditions on microstructural development and phase transformation in silicon carbide, J. Am. Ceram. Soc. 83 (6) (2000) 1369–1374.
[15] S.-G. Lee, Y.-W. Kim, M. Mitomo, Relationship between microstructure and fracture toughness of toughened silicon carbide ceramics, J. Am. Ceram. Soc. 86 (6) (2001) 1347–1353.
[16] T. Mitchell Jr., L.C. De Jonghe, W.J. MoberlyChan, R.O. Ritchie, Silicon carbide platelet/silicon carbide composites, J. Am. Ceram. Soc. 78 (1) (1995) 97–103.
[17] S.-H. Kim, Y.-W. Kim, M. Mitomo, Microstructure and fracture toughness of liquid-phase-sintered β-SiC containing β-SiC whiskers as seeds, J. Mater. Sci. 38 (2003) 1117–1121.
[18] K. Suzuki, N. Kageyama, K. Furukawa, T. Kanno, Oxidation of sintered silicon carbide with addition of aluminium oxide, in: W. Bunk, H. Hausner (Eds.), Proceedings of Second International Symposium on Ceramic Materials and Components for Engines, SDV GmbH, Saarbrucken, 1986, pp. 697–704.
[19] S.S. Shinozaki, J. Hangas, K.R. Carduner, M.J. Rokosz, K. Suzuki, N. Shinohara, Correlation between microstructure and mechanical properties in silicon carbide with alumina addition, J. Mater. Res. 8 (7) (1993) 1635–1643.
[20] K. Suzuki, Silicon carbide-aluminum nitride sintered article and process for its production (Asahi Glass Co., Ltd.), US patent 4569922, 11 February 1986.
[21] I.B. Cutler, P.D. Miller, W. Rafaniello, H.K. Park, D.P. Thompson, K.H. Jack, New materials in the Si–C–Al–O–N and related systems, Nature 275 (1978) 434–435.
[22] W. Rafaniello, K. Cho, A.V. Virkar, Fabrication and characterization of SiC–AlN alloys, J. Mater. Sci. 16 (1981) 3479–3488.
[23] W.-C.J. Wei, R.-R. Lee, Pressureless sintering of AlN–SiC composites, J. Mater. Sci. 26 (1991) 2930–2936.
[24] M. Ohyanagi, K. Shirai, N. Balandina, M. Hisa, Z.A. Munir, Synthesis of aluminum nitride–silicon carbide solid solutions by combustion nitridation, J. Am. Ceram. Soc. 83 (5) (2000) 1108–1112.
[25] K. Nakamura, K. Maeda, Hot-pressed SiC ceramics, in: S. Somiya, Y. Inomata (Eds.), Silicon Carbide Ceramics—2, Elsevier Applied Science, London and New York, 1991, pp. 139–162.
[26] Y.-W. Kim, M. Mitomo, T. Nishiyama, Heat-resistant silicon carbide with aluminum nitride and erbium oxide, J. Am. Ceram. Soc. 84 (9) (2001) 2060–2064.
[27] Y.-W. Kim, K. Ando, M.C. Chu, Crack-healing behavior of liquid-phase-sintered silicon carbide ceramics, J. Am. Ceram. Soc. 86 (3) (2003) 465–470.
[28] Japanese Industrial Standard, R 1607, Testing methods for fracture toughness of fine ceramics (1995).
[29] Y.-W. Kim, M. Mitomo, Fine-grained silicon carbide ceramics with oxynitride glass, J. Am. Ceram. Soc. 82 (10) (1999) 2731–2736.
[30] H.-W. Jun, H.-W. Lee, G.-H. Kim, H.-S. Song, B.-H. Kim, Effect of sintering atmosphere on the microstructure evolution and mechanical properties of silicon carbide ceramics, Ceram. Eng. Sci. Proc. 18 (4) (1997) 487–504.
[31] Y. Tajima, W.D. Kingery, Solid solubility of aluminum and boron in silicon carbide, J. Am. Ceram. Soc. 65 (2) (1982) 27–29.
[32] T. Nagano, K. Kaneko, G.-D. Zahn, M. Mitomo, Effect of atmosphere on weight loss in sintered silicon carbide during heat treatment, J. Am. Ceram. Soc. 83 (11) (2000) 2781–2787.